Available online at www.sciencedirect.com

SciVerse ScienceDirect

Ceramics International 38 (2012) 6377–6387

CERAMICS INTERNATIONAL

www.elsevier.com/locate/ceramint

Electrochemical decomposition of CO_2 and CO gases using porous yttria-stabilized zirconia cell

Yoshihiro Hirata*, Masahiro Ando, Naoki Matsunaga, Soichiro Sameshima

Department of Chemistry, Biotechnology, and Chemical Engineering, Kagoshima University, 1-21-40 Korimoto, Kagoshima 890-0065, Japan

Received 14 March 2012; accepted 4 May 2012
Available online 12 May 2012

Abstract

Electrochemical decomposition of CO_2 and CO gases using a porous cell of Ru-8 mol% yttria-stabilized zirconia (YSZ) anode/porous YSZ electrolyte/Ni–YSZ cathode system at 400–800 °C was studied by analyzing the flow rate and composition of outlet gas, current density, and phases and elementary distribution of the electrodes and electrolyte. A part of CO_2 gas supplied at 50 ml/min was decomposed to solid carbon and O_2 gas through the cell at the electric field strengths of 0.9–1.0 V/cm. The outlet gas at a flow rate of 3 ml/min included 61–63% CO_2 and 37–39% O_2 at 700–800 °C and the outlet gas at a flow rate of 50 ml/min included 73–96% (average 85%) CO_2 and 4–27% (average 15%) O_2 at 800 °C. On the other hand, the supplied CO gas was also decomposed to solid carbon, O_2 and CO_2 gases at 800 °C. The fraction of outlet gas at a flow rate of 50 ml/min during the CO decomposition at 800 °C for 5 h was 11–36% CO, 59–81% O_2 and 2–9% CO_2. The detailed decomposition mechanisms of CO_2 and CO gases are discussed. Both Ni metal in the cathode and porous YSZ grains under the DC electric field have the ability to decompose CO gas into solid carbon and O^{2-} ions or O_2 gas.

Keywords: A. Sintering; C. Chemical properties; D. Carbon; D. ZrO_2

1. Introduction

It is well recognized that the concentration of CO_2 in atmosphere increases since the end of 18th century because of the consumption of a large amount of coal, oil and natural gas and this phenomenon causes a serious problem of global warming. On the other hand, the following photosynthesis by plants produces grape sugar, H_2O and O_2 gas from CO_2 and H_2O: $12H_2O+6CO_2+\text{photoenergy}\rightarrow C_6H_{12}O_6$ (grape sugar)$+6H_2O+6O_2$. (1) This photosynthesis process is ideal to reduce the amount of CO_2 gas. However, no commercial system of artificial photosynthesis is established at this moment. Sayama et al. [1] reported stoichiometric decomposition of water into H_2 and O_2 under visible light (wavelength > 420 nm) using a mixture of two different photocatalysts of Pt–WO_3 and Pt–$SrTiO_3$ (Cr–Ta-doped) in NaI aqueous solution (IO_3^-/I^- shuttle redox mediator). The photocatalytic reaction proceeds as follows: $6H^+ + 6e^- \rightarrow 3H_2$ (conduction band of Pt–$SrTiO_3$ (Cr–Ta doped)), $I^- + 6OH^- + 6h^+ \rightarrow IO_3^- + 3H_2O$ (valence band of Pt–$SrTiO_3$ (Cr–Ta doped)), $IO_3^- + 3H_2O + 6e^- \rightarrow I^- + 6OH^-$ (conduction band of Pt–WO_3), $6OH^- + 6h^+ \rightarrow 3/2O_2 + 3H_2O$ (valence band of Pt–WO_3). The rates of H_2 and O_2 evolution under monochromatic light (420.7 nm wavelength, 57 mW) were 0.21 and 0.11 μmol/h, respectively. The quantum efficiency is estimated to be 0.1%. Sato et al. [2] also developed an artificial photosynthesis system (CO_2 conversion to formate) under visible light (wavelength > 400 nm) using two types of different photocatalysts: zinc-doped indium phoshide (InP) plus ruthenium complex polymer for the reduction of CO_2 ($CO_2 + H^+ + 2e^- \rightarrow HCOO^-$) and Pt–$TiO_2$ for the oxidation of water ($H_2O \rightarrow 2H^+ + 1/2O_2 + 2e^-$) in 10 mM $NaHCO_3$ aqueous solution. The formation rate and selectivity of HCOOH was 0.229 μmol/cm^2/h and 70%, respectively. However, more high rate systems for the conversion of CO_2 gas and H_2O are needed to suppress global warming.

Recently, our group developed the electrochemical cells of Ru–Gd-doped ceria (GDC) anode/porous GDC electrolyte/Ni or Ru–GDC cathode system [3–5] and

*Corresponding author. Tel.: +81 99 285 8325; fax: +81 99 257 4742.
E-mail address: hirata@apc.kagoshima-u.ac.jp (Y. Hirata).

0272-8842/$36.00 © 2012 Elsevier Ltd and Techna Group S.r.l. All rights reserved.
http://dx.doi.org/10.1016/j.ceramint.2012.05.010

Ru-8 mol% yttria-stabilized zirconia (YSZ) anode/porous YSZ electrolyte/Ni–YSZ cathode system [6] to reform biogas (mixed gas of 30–70 vol% CH_4 and 70–30 vol% CO_2). These cells work well under a small electric field strength of 1–2 V/cm at 400–800 °C. The supplied CO_2 is changed to CO and O^{2-} ions by the reaction with electrons at the cathode ($CO_2+2e^-\rightarrow CO+O^{2-}$). The produced CO and O^{2-} ions are transported to the anode through a porous GDC or YSZ film. In the anode, CH_4 reacts with O^{2-} ions to produce CO, H_2 and electrons ($CH_4+O^{2-}\rightarrow CO+2H_2+2e^-$). Especially, the Ru–GDC anode/porous GDC electrolyte/ Ni–GDC cathode system changed well biogas above 90% to form H_2 and CO gases at 800 °C ($CH_4+CO_2\rightarrow 2H_2+2CO$). The structures and functional characteristics of the developed cells are different from solid oxide fuel cell (SOFC) system using a dense electrolyte which separates completely the supplied fuel (anode) and air (cathode). According to the literature survey at 1993–2009, no electrochemical system using a porous electrolyte cell has been reported for the reforming of biogas. Furthermore, we challenged in this paper to decompose highly concentrated CO_2 and CO gases through the developed porous YSZ cell at 400–800 °C. This experiment provided a remarkable result like photosynthesis by plants. That is, both CO_2 and CO gases were decomposed to solid carbon and O_2 gas through the porous electrochemical cell. This paper reports the fraction of reformed gas, carbon deposition in the cell and decomposition mechanisms of CO_2 and CO. The attractive point of this result is the greatly high decomposition rates of CO_2 and CO, which contribute to suppress global warming.

2. Experimental procedure

2.1. Preparation of electrochemical cell

The detailed preparation method of the porous electrochemical cells is reported in our previous papers [3–6]. The supplied 8 mol% yttria-stabilized zirconia (YSZ) powder (Tosoh Co. Ltd., Japan, ZrO_2 86.27 mass%, Y_2O_3 13.64 mass%, Al_2O_3 0.005 mass%, SiO_2 0.007 mass%, Fe_2O_3 0.003 mass% and Na_2O 0.074 mass%, specific surface area 13.3 m^2/g) was immersed into a 1.4 M $Ni(NO_3)_2$ solution or 0.2 M $RuCl_3$ solution to make a cermet cathode or anode with a volume ratio of Ni or Ru:YSZ = 30:70. The $RuCl_3$–YSZ suspension was adjusted to pH 10 using a 13 M NH_4OH solution to prepare Ru hydroxide on YSZ particles. These suspensions were stirred for 6 h and then freeze-dried. The freeze-dried powders were calcined at 600 °C (NiO–YSZ powder) or 800 °C (RuO_2–YSZ powder) for 1 h in air and further heated at 1000 °C for 2 h in air to form a porous structure of electrode. The supplied YSZ particles (isoelectric point pH 2.8 [7]) were also agglomerated at pH 3 and heated at 1000 °C for 2 h to promote its grain growth, which is effective to achieve a porous structure of electrolyte layer. The layer of heated YSZ powder was sandwiched with the layers of cathode and anode powders, and the three layers were pressed uniaxially at 50 MPa for 1 min, followed by isostatic pressing at 100 MPa for 1 min. The layered compact was sintered at 800 °C (experiment A) or 900 °C (experiment B) for 2 h in air. The thickness of cathode, electrolyte and anode was 5, 1 and 5 mm, respectively.

2.2. Electrochemical decomposition of CO_2 and CO

Pt meshes were attached to both the electrodes using Pt paste. The electrochemical cell sintered in air was set to an alumina holder and sealed at 870 °C for 10 min by using a glass O-ring (HV10R, Iwaki Glass Co., Japan, chemical composition (mass%)-81 SiO_2, 2 Al_2O_3, 13 B_2O_3, 4 Na_2O–K_2O) and glass powder (ASF1761, Asahi Glass Co. Ltd., Japan, chemical composition (mass%)-50–70SiO_2, 2–15BaO, 2.5B_2O_3, 2–15Al_2O_3, 2–15CaO, 1–10ZrO_2). After cooling to 700 °C, a 3 vol% H_2O-containing H_2 gas was fed into the cell at 50 ml/min for 24 h to reduce NiO and RuO_2 to Ni and Ru, respectively. The relative densities of porous electrodes were measured by the Archimedes method using distilled water. Then, the electrochemical cell of Ru (30 vol%)–YSZ anode/YSZ electrolyte/Ni (30 vol%)–YSZ cathode system was cooled down to 400 °C and 1 V of external voltage was applied by potentiostat (HA-501 G, Hokuto Denko Co., Japan). CO_2 gas (purity > 99.99%) was fed at 50 ml/min into the cathode of electrochemical cell operated at 400–800 °C (Fig. 1). The composition of outlet gas was analyzed by gas chromatography (GT 3800, Yanaco Co., Japan) with active carbon (60/80 mesh) using a thermal conductivity detector at 100 °C. The outlet gas of 0.2 ml was injected into an Ar carrier gas at 100 °C. Similarly, the mixed gas of 10 vol% CO-90 vol% Ar system was fed at 50 ml/min into the porous YSZ cell. The heating temperature of the cell was changed from a high temperature (800 °C) to a low temperature (400 °C) to avoid disproportionation of CO ($2CO\rightarrow CO_2+C$) which occurs below 600 °C [5]. The composition of outlet gas during CO decomposition was analyzed by gas chromatography (GC7100T, J-Science Lab Co. Ltd. Japan) with active carbon (60/80 mesh) and MS-5A (60/80 mesh) using a thermal conductivity detector at 120 °C. The outlet gas of 2 ml was introduced into an Ar carrier gas at 120 °C through gas sampler. Phase identification of Ru–YSZ anode and Ni–YSZ cathode before and after the decomposition of CO_2 and CO was carried out using X-ray diffraction (RINT 2200PCH/KG, Rigaku Co., Japan). Elementary distribution of C, O, Ni, Y, Zr and Ru of cross section of the porous YSZ cell after the decomposition of CO_2 and CO was measured by electron probe microanalyzer (EPMA, JXA-8230, JEOL Ltd., Japan).

3. Results and discussion

3.1. Electrochemical decomposition of CO_2

Typical open porosities of Ru–YSZ anode, porous YSZ electrolyte and Ni–YSZ cathode after the reaction with a

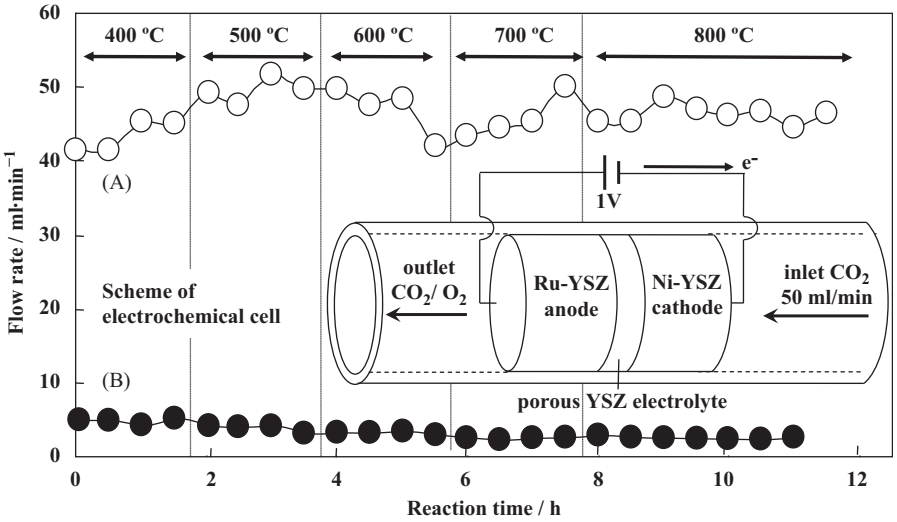

Fig. 1. Scheme of the porous electrochemical cell of Ru-8 mol% Y_2O_3-stabilized zirconia (YSZ) anode/YSZ/Ni–YSZ cathode system and time dependence of flow rate of outlet gas during CO_2 decomposition. Experiments were carried out two times (A, B) using electrochemical cells sintered at 800 °C (experiment A) and 900 °C (experiment B).

H_2 gas at 700 °C were 64.4, 55.7 and 57.0%, respectively. These values were similar to the open porosities of the anode (65.9%), YSZ electrolyte (55.7%) and the cathode (65.9%) in previous experiment [6]. Fig. 1 shows the scheme of porous electrochemical cell and time dependence of flow rate of outlet gas through the YSZ cell at 400–800 °C during CO_2 decomposition. The experiment was carried out two times (A, B) using different electrochemical cells sintered at 800 °C (experiment A) and 900 °C (experiment B). In cell B, RuO_2–YSZ anode powder and NiO–YSZ cathode powder were only calcined at 1000 °C for 1 h before the sintering. No significant change of flow rate was measured above 10 h of reaction time for 1st experiment (A), indicating little blockage of inlet gas at the flow rate of 50 ml/min. Similarly, little time dependence of flow rate of outlet gas was measured for 2nd experiment (B) but the flow rate for experiment (B) decreased to 2.3–5.2 ml/min. The difference in pore structures of the produced two cells may affect the result in Fig. 1. Increased sintering temperature for cell B leads to the decrease of open porosity and pore size, resulting in the decreased flow rate of outlet gas [4]. Fig. 2 shows the average current density of electrochemical cells in experiments (A) and (B). The current density was small at 400–500 °C but increased drastically above 500 °C. This result is explained by the increased oxide ion conductivity of YSZ electrolyte at a higher temperature. The oxide ions are supplied from CO_2 at the cathode ($CO_2+2e^- \rightarrow CO+O^{2-}$). Fig. 3 shows the fraction of outlet gas through the electrochemical cell operated at 0.91 V/cm. The outlet gas for both experiments (A) and (B) at 400–800 °C included CO_2 and O_2 gases and no CO gas was formed. This result was different from the reforming of the CH_4–CO_2 mixed gas, which provided the outlet gas of H_2–CO system. The CO_2 and O_2 fractions in Fig. 3 were 73–96%

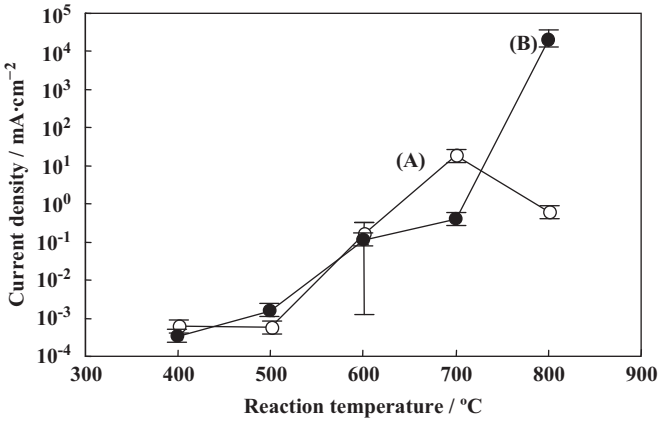

Fig. 2. Current density of the porous YSZ cells operated at 0.91 V/cm during CO_2 decomposition experiments (A, B) at 400–800 °C.

(average 85%) and 4–27% (average 15%) for experiment (A) at 800 °C, and 61 and 39% for experiment (B) at 800 °C, respectively. When the flow rate of outlet gas was low, the O_2 fraction became higher. A similar tendency was also measured in the reforming of the CH_4–CO_2 mixed gas. The conversion ratio of CO_2 (or CH_4) of inlet gas became higher at a lower open porosity in our previous experiment [6]. When the pore size is small, the mean free path of CO_2 becomes shorter, enhancing collision frequency between CO_2 and Ni particles [4]. The increased collision frequency leads to the high reforming efficiency of CO_2. The analysis of gas composition in Fig. 3 suggests the possibility of electrochemical decomposition of CO_2 into C plus O_2. This reaction is supported by the following analysis of the YSZ cell.

Fig. 4 shows the X-ray diffraction patterns of Ni–YSZ cathode and Ru–YSZ anode after CO_2 decomposition at 800 °C for experiment (A). As seen in Fig. 4, NiO and

RuO_2 were identified at cathode and anode, respectively. A small amount of Ni was also identified on the cross section of the inside of cathode. The diffraction peaks of Pt come from the Pt paste to attach Pt wires to the cell. That is, the Ni and Ru metals in the electrodes were oxidized during CO_2 decomposition. The detailed reaction mechanisms are discussed in a later part (Fig. 6).

Fig. 5 shows the elementary distribution at the boundary between YSZ electrolyte and Ni–YSZ cathode after the CO_2 decomposition at 800 °C. The distribution map of Zr overlapps that of Y, indicating the formation of YSZ solid solution. The distribution map of Ni is out of accordance with that of Zr, indicating the phase compatibility between Ni and YSZ. An interesting observation is the formation of C near the areas of Ni and Zr but the area of C overlapps scarcely the distribution maps of YSZ electrolyte and NiO. This result suggests that the boundary of Ni and YSZ accelerates CO_2 decomposition. Fig. 5(g) shows the energy dispersive X-ray spectra at the Ni–YSZ cathode. The formation of C is also confirmed by the clear spectrum of C at 0.26 keV. The X-ray spectra for Na result from the glass O-ring used to attach the cell to an alumina holder.

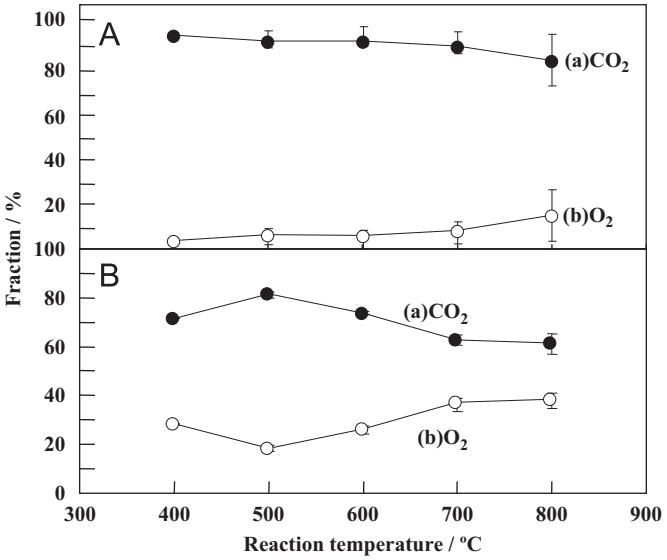

Fig. 3. Fraction of outlet gas through the porous YSZ cells (A, B) during CO_2 decomposition at 400–800 °C.

Figs. 6 and 7 show the energy dispersive X-ray spectra at the porous YSZ electrolyte and Ru–YSZ anode, respectively, after the CO_2 decomposition at 800 °C. In addition to Y, Zr and O elements, the deposition of C is clearly presented. The amount of deposited carbon was high in the cathode (Fig. 5) and low in the YSZ electrolyte and anode. The spectra for Al and Na are due to the glass O-ring (HV10R, Iwaki Glass Co., Japan) and glass powder (ASF1761, Asahi Glass Co. Ltd., Japan) to attach the cell to an alumina holder.

Based on the results in Figs. 1–7, a possible decomposition mechanism for CO_2 at the cathode is proposed in Fig. 8. Ni metal at the cathode reacts with CO_2 to form NiO and CO gas by Eq. (2). The formed NiO is decomposed to Ni and O^{2-} ions by reaction with the supplied electrons (Eq. (3)). The produced O^{2-} ions are transported to the anode by surface diffusion and bulk diffusion through YSZ electrolyte (oxide ion conductor). Ni metal in Eq. (3) and CO gas in Eq. (2) react further to form NiO and solid C. The summation of Eqs. (2)–(4) provides Eq. (5). The above reaction mechanism explains well the formation of NiO and C at the boundary of NiO and YSZ in the cathode in Fig. 5.

The two reactions by Eqs. (6) and (7) are possible to separate the electrons on oxide ions in the anode. A part of transported O^{2-} ions (fraction:x) reacts with Ru to form

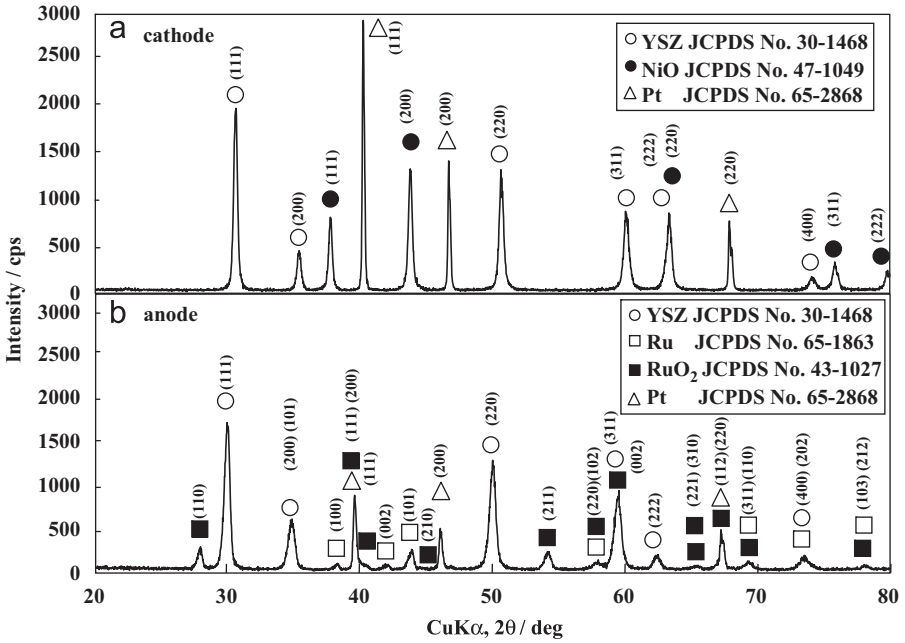

Fig. 4. X-ray diffraction patterns of (a) Ni–YSZ cathode and (b) Ru–YSZ anode after CO_2 decomposition experiment (A) at 800 °C.

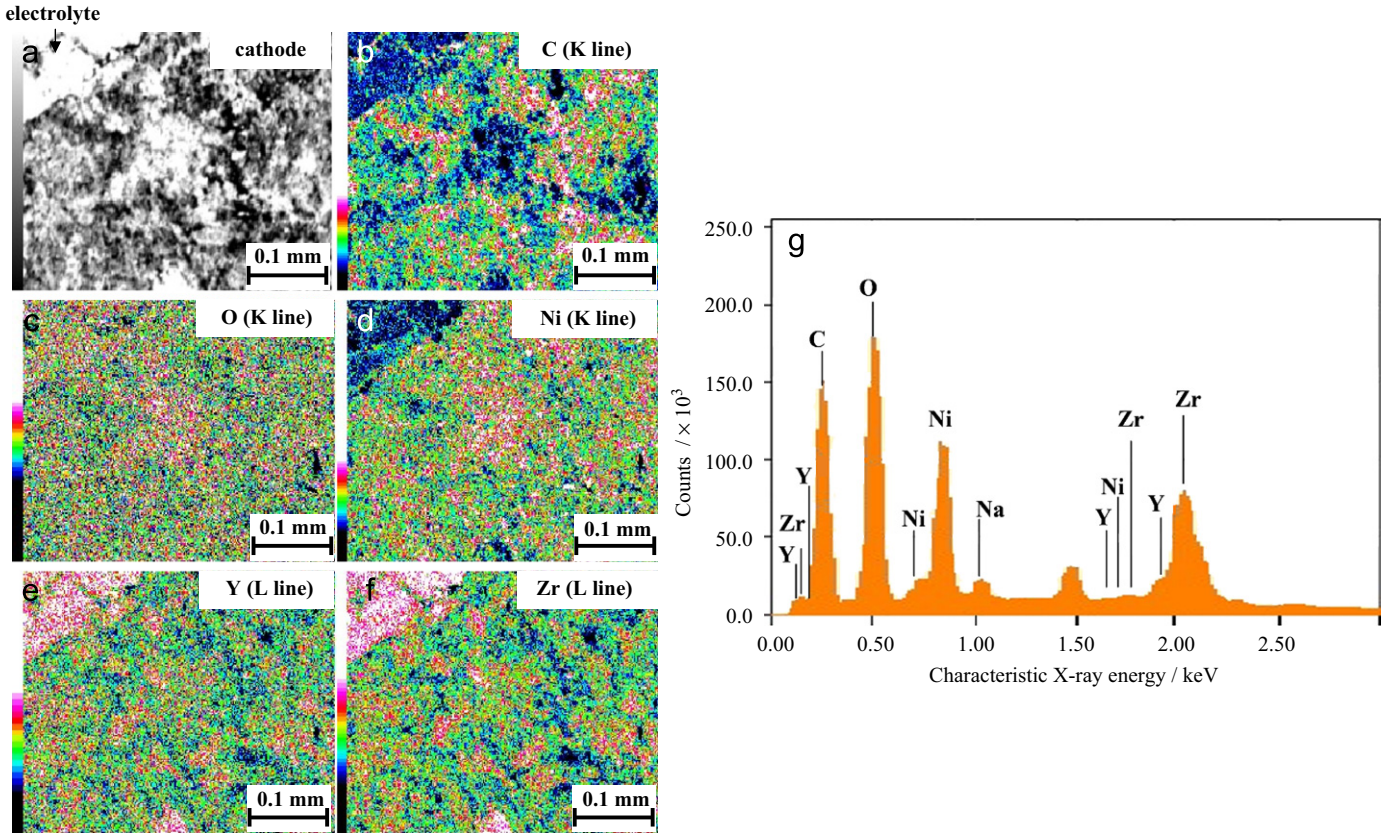

Fig. 5. (a) Microstructure of the boundary region between YSZ electrolyte and Ni–YSZ cathode after CO_2 decomposition at 800 °C, elementary distribution map of (b) C (K line), (c) O (K line), (d) Ni (K line), (e) Y (L line) and (f) Zr (L line), and (g) energy dispersive X-ray spectra at the Ni–YSZ cathode.

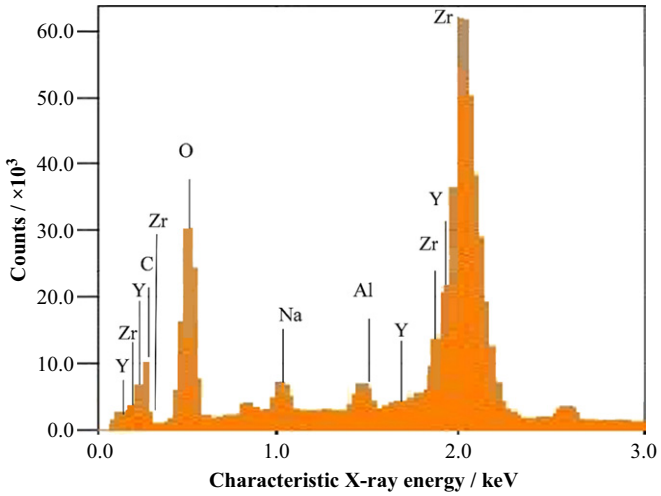

Fig. 6. Energy dispersive X-ray spectra at the YSZ electrolyte after CO_2 decomposition at 800 °C for 5 h.

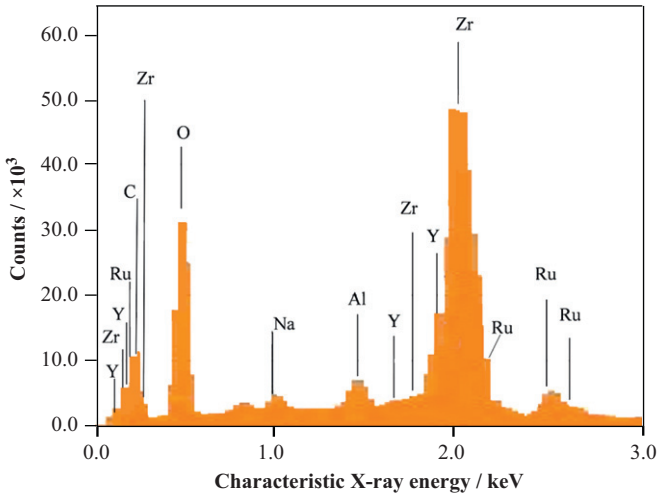

Fig. 7. Energy dispersive X-ray spectra at the Ru–YSZ anode after CO_2 decomposition at 800 °C for 5 h.

RuO_2 by Eq. (6). The remaining O^{2-} ions change to O_2 gas and electrons by Eq. (7). The summation of Eqs. (6) and (7) provides Eq. (8), which explains well the formation of RuO_2 and O_2 gas in the anode. Equation (9) represents the total reaction for CO_2 decomposition in the porous YSZ cell. In the case of $x=0$, CO_2 reacts with Ni to form O_2, C and NiO. The case of $x=1$ expresses the interaction between CO_2 gas and the electrodes to form NiO, RuO_2 and C.

In addition to the reaction expressed by Eq. (9), another parallel reaction occurs to produce CO_2 gas in Fig. 3. The coupling of Eqs. (2) and (3) provides Eq. (10).

$$2CO_2 + 4e^- \rightarrow 2CO + 2O^{2-} \quad (10)$$

The produced CO gas and O^{2-} ions are transported to the anode. The oxide ions in the anode react with Ru metal to form RuO_2 by Eq. (6) in Fig. 8.

Cathode

$2Ni + 2CO_2 \rightarrow 2NiO + 2CO$ (2)

$2NiO + 4e^- \rightarrow 2Ni + 2O^{2-}$ (3)

$2Ni + 2CO \rightarrow 2NiO + 2C$ (4)

(2)+(3)+(4) $2Ni + 2CO_2 + 4e^- \rightarrow 2NiO + 2C + 2O^{2-}$ (5)

Anode (I) $xRu + 2xO^{2-} \rightarrow xRuO_2 + 4xe^-$ (6)

Anode (II) $2\,(1-x)\,O^{2-} \rightarrow (1-x)\,O_2 + 4\,(1-x)\,e^-$ (7)

(6)+(7) $xRu + 2O^{2-} \rightarrow xRuO_2 + (1-x)O_2 + 4e^-$ (8)

Total, (5)+(8) $2CO_2 + 2Ni + xRu \rightarrow (1-x)O_2 + 2C + 2NiO + xRuO_2$ (9)

Fig. 8. Electrochemical decomposition mechanism of CO_2 gas through porous YSZ cell.

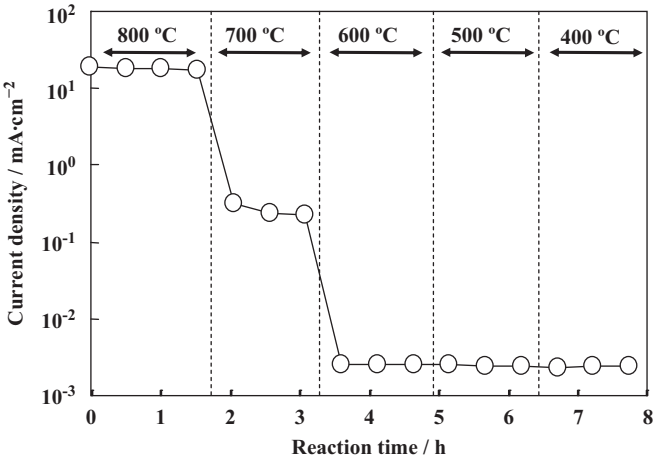

Fig. 9. Current density of the porous YSZ cell operated at 1.0 V/cm during CO decomposition at 800–400 °C.

$$Ru + 2O^{2-} \rightarrow RuO_2 + 4e^- \quad (6)$$

RuO_2 is also reduced by CO gas transported to form Ru and CO_2 by Eq. (11).

$$RuO_2 + 2CO \rightarrow Ru + 2CO_2 \quad (11)$$

The combination of above reactions by Eqs. (10), (6) and (11) provides Eq. (12).

$$2CO_2 + 4e^- \rightarrow 2CO_2 + 4e^- \quad (12)$$

This equation explains the coexistence of O_2 and CO_2 gases. The deposition mechanism of solid C in the porous electrolyte and the anode is discussed in Section 3.3.

3.2. Electrochemical decomposition of CO

The electrochemical cell with open porosities of 67.7% for Ru–YSZ anode, 55.7% for YSZ electrolyte and 54.7% for Ni–YSZ cathode was used for the decomposition of CO gas. CO gas is usually produced from the reforming of CH_4–CO_2 mixed gas ($CH_4 + CO_2 \rightarrow 2H_2 + 2CO$) or reaction of Fe–$CO_2$ system ($4CO_2 + 3Fe \rightarrow Fe_3O_4 + 4CO$). As described in Section 2.2, the cell temperature was changed from 800 °C to 400 °C to avoid disproportionation of CO ($2CO \rightarrow CO_2 + C$) at a lower temperature [5]. When a 10% CO-90% Ar mixed gas was fed at 50 ml/min into the cathode of porous cell, no change of the flow rate and no blockage of the inlet gas were measured at 800–400 °C. Fig. 9 shows the current density during the electrochemical decomposition of CO gas. The current density was higher at a higher cell temperature. This tendency was similar to that measured for the decomposition of CO_2 in Fig. 2 and may be explained by the higher oxide ion conductivity of porous YSZ electrolyte at a higher temperature. Fig. 10 shows the fraction of outlet gas through the electrochemical cell operated at 1.0 V/cm. The outlet gas included CO, O_2 and CO_2 gases in the wide temperature range. The reaction at 800 °C produced a large amount of O_2 gas (67–80%). The detailed reaction mechanisms are discussed in a later part. In the temperature range of 700–400 °C, the fraction of O_2 gas decreased drastically and the fraction of CO_2 increased at 500–400 °C. The result at 500–400 °C is related to the disproportionation of CO gas ($2CO \rightarrow CO_2 + C$). Fig. 11 shows the X-ray diffraction patterns of Ni–YSZ cathode and Ru–YSZ anode after the CO decomposition at 800–400 °C. Only Ni, Ru and YSZ were identified and no oxide compounds of Ni and Ru were recognized. This result is different from the oxidation of Ni and Ru in the electrodes during the CO_2 decomposition (Fig. 4).

Fig. 12 shows the C content of the cell after the CO decomposition experiment at 800–400 °C. The measured C content was referred to 100% carbon material. The deposited carbon was 14–19 mass% at Ni–YSZ cathode, 8–10 mass% at YSZ electrolyte and 10–12 mass% at Ru–YSZ anode, respectively. This result includes the information of C deposition by disproportionation of CO at 500–400 °C. However, the formation of O_2 gas at 800 °C in Fig. 10 suggests the possibility of another formation mechanism of C: the direct decomposition of CO into C and O_2 through the electrochemical cell. To confirm this possibility, CO gas was fed into the porous YSZ cell for 5 h at 800 °C. Then, the cell atmosphere was substituted for a high purity Ar gas (oxygen partial pressure: 10^{-17} Pa) and

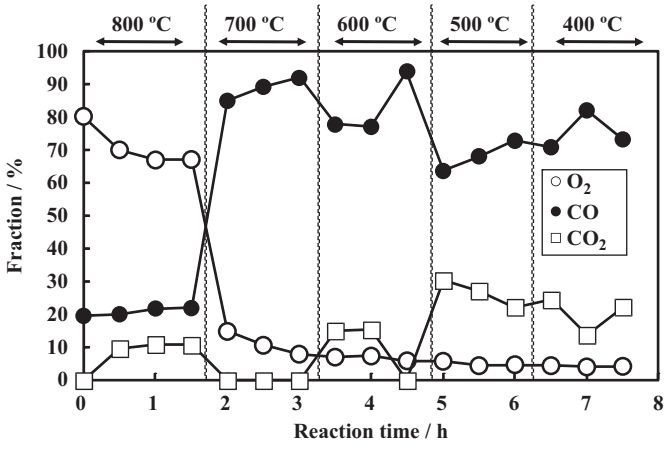

Fig. 10. Fraction of outlet gas through the porous YSZ cell operated at 1.0 V/cm during CO decomposition.

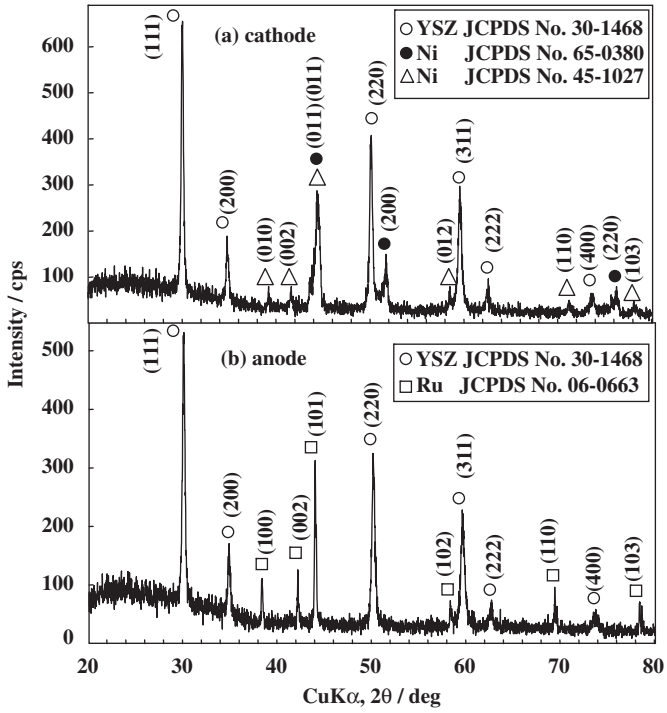

Fig. 11. X-ray diffraction patterns of (a) Ni–YSZ cathode and (b) Ru–YSZ anode after CO decomposition at 800–400 °C.

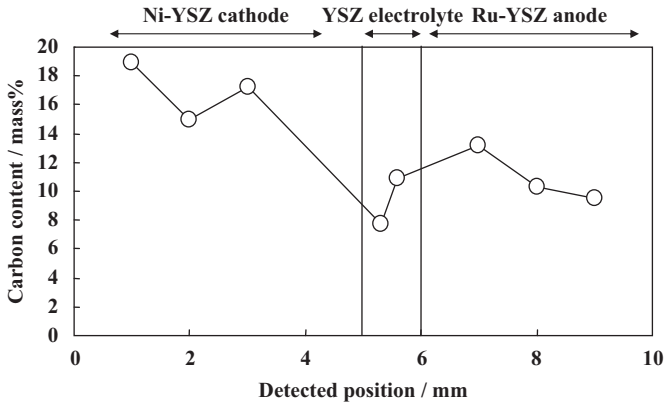

Fig. 12. Carbon content in the porous YSZ cell after CO decomposition at 800–400 °C.

cooled to room temperature to avoid the influence of disproportionation of CO at lower temperatures.

Fig. 13 shows the fraction of outlet gas through the electrochemical cell operated at 1.0 V/cm at 800 °C. The outlet gas included 11–36% CO, 59–81% O_2 and 2–9% CO_2 gas and the fraction of O_2 gas decreased gradually with increasing reaction time. This result suggests also the possibility of decomposition of CO into C and O_2 gas.

Figs. 14 and 15 show the elementary distribution of cathode and anode, respectively, for the YSZ cell operated in a CO atmosphere at 800 °C for 5 h and cooled in an Ar atmosphere. In Fig. 14, carbon deposition is clearly observed (b) and its area does not overlap the areas of Ni and YSZ (d–f). The energy dispersive X-ray spectra in Fig. 14(g) indicate apparently the formation of carbon.

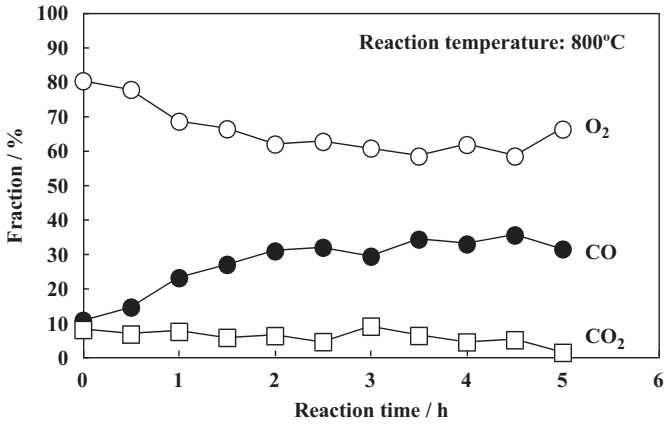

Fig. 13. Fraction of outlet gas through the porous YSZ cell operated at 800 °C for 5 h.

The spectra for Al and Si come from the metal Al evaporated to the microstructural observation and a glass O-ring (HV10R, Iwaki Glass Co., Japan) and glass powder (ASF1761, Asahi Glass Co. Ltd., Japan) used to attach the cell to an alumina holder. Similarly, carbon deposition is also measured in the anode in Fig. 15. The carbon area (b) does not overlap the areas of Ru and YSZ (d–f). The energy dispersive X-ray spectra in Fig. 15(g) also support the formation of C in the anode. Therefore, the results in Figs. 12–15 lead to the conclusion that CO gas was decomposed to C and O_2 gas through the porous YSZ cell at 800 °C.

Fig. 16 shows the possible decomposition mechanism of CO gas at 800 °C. In the cathode, CO gas reacts with Ni to form NiO and C by Eq. (13). The formed NiO reacts again with supplied electrons to produce Ni and O^{2-} ions by Eq. (14). The above two reactions are same mechanism as Eqs. (3) and (4) in Fig. 8. The summation of Eqs. (13) and (14) provides Eq. (15), which explains no oxidation of Ni measured in Fig. 11. The formed O^{2-} ions are transported to the anode by surface diffusion and bulk diffusion through the YSZ electrolyte. Equations (16)–(18) show the two possible reactions at the anode to separate electrons from the transported oxide ions. Equation (16) expresses the formation of O_2 gas from oxide ions. Another reaction with oxide ions is expressed by Eq. (17). However, no formation of RuO_2 was recognized in Fig. 11(b). The formed RuO_2 reacts with the conveyed CO gas to produce Ru and CO_2 gas. Summation of Eqs. (17) and (18) provides Eq. (19), which explains well no oxidation of Ru in the anode and the formation CO_2 gas at 800 °C in Figs. 10 and 13. When both the reactions of Eqs. (16) and (19) occur at the fractions of y and $1-y$ of the amount of transported O^{2-} ions, respectively, the total reaction at the anode is represented by Eq. (20). Finally, the coupling of Eqs. (15) and (20) provides the electrochemical decomposition of CO by Eq. (21). The case of $y=0$ in Eq. (21) results in the reaction of $4CO \rightarrow 2C+2CO_2$. This equation expresses the disproportionation of CO. On the other hand, the case of $y=1$ results in the

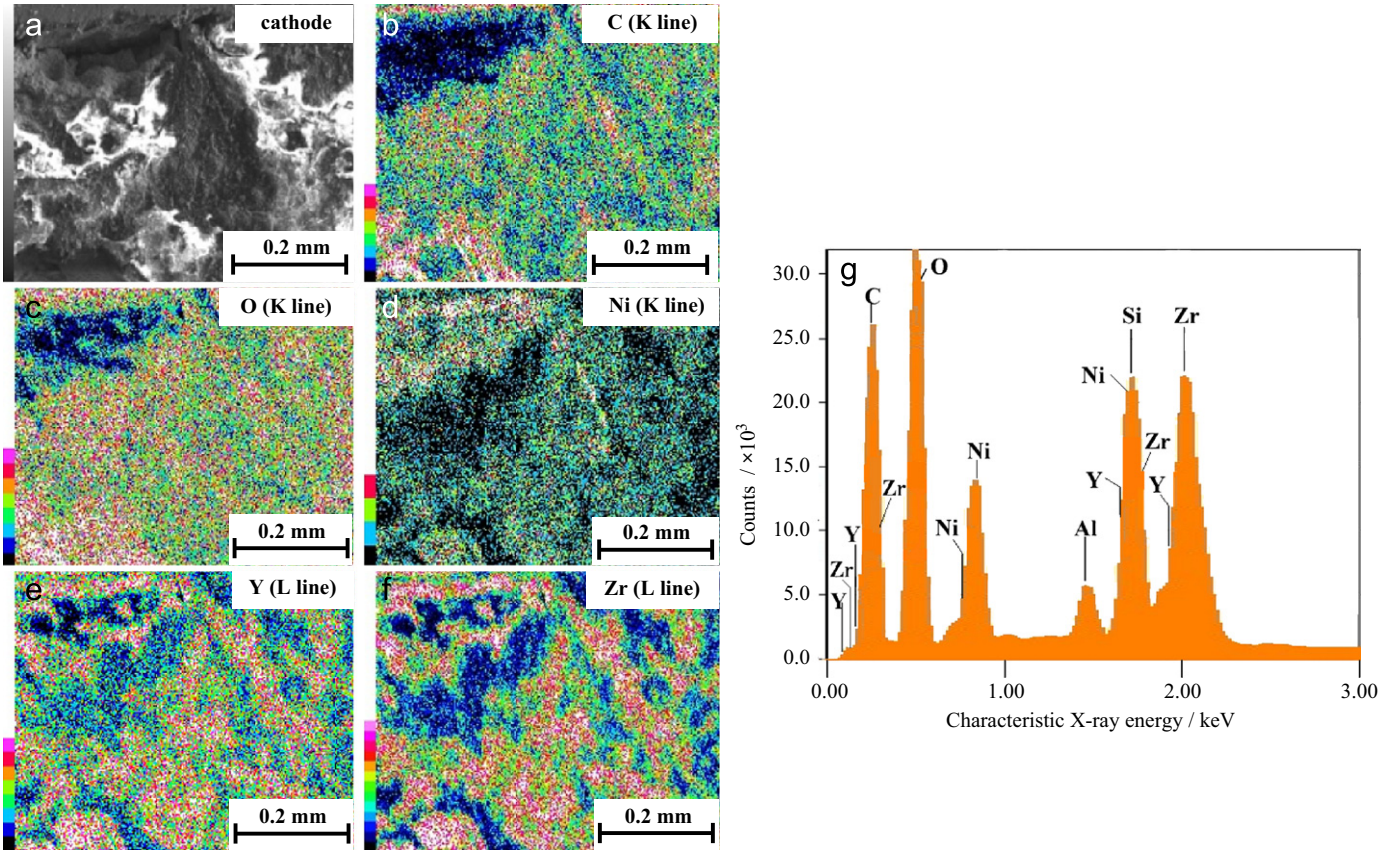

Fig. 14. (a) Microstructure of the Ni–YSZ cathode after CO decomposition at 800 °C for 5 h, elementary distribution map of (b) C (K line), (c) O (K line), (d) Ni (K line), (e) Y (L line) and (f) Zr (L line), and (g) energy dispersive X-ray spectra at the Ni–YSZ cathode.

direct decomposition of CO into C and O_2 gas. The formation mechanism of C in Fig. 16 succeeds in explaining the result at the cathode in Fig. 14. However, the reaction mechanism in Fig. 16 does not explain the carbon deposition at the anode in Fig. 14. To clarify another formation mechanism of carbon deposition, we analyzed the elementary distribution at the porous YSZ electrolyte after the CO decomposition experiment in Fig. 13. This result is discussed in a next section.

3.3. Electrochemical decomposition of CO gas over YSZ grains under DC field

Fig. 17 shows the elementary distribution of the porous YSZ electrolyte after the CO decomposition experiment in Fig. 13. It is clearly observed that carbon is deposited around YSZ solid solution grains (b). The enriched concentration of oxygen (c) is also observed near the area of carbon deposition. The energy dispersive X-ray spectra in Fig. 17(f) indicate the deposition of C in the porous YSZ electrolyte. The spectra for Na, Al and Si are due to the glass powder and glass O-ring to attach the YSZ cell to an alumina holder. Fig. 18 shows the scheme of CO decomposition mechanism over YSZ grains based on the result measured in Fig. 17. The substitution of Zr^{4+} ions for Y^{3+} ions produces the positively charged oxygen vacancy by Eq. (22). The supplied CO gas reacts with the oxygen vacancy to form solid C and positively charged holes by Eq. (23). However, little hole conduction occurs in the YSZ electrolyte under low oxygen partial pressures. The produced holes react quickly with oxide ions transported by surface diffusion and bulk diffusion through YSZ grains from the cathode (Eq. (15) in Fig. 16). As a result, oxygen gas is produced over YSZ grains by Eq. (24). Equation (25) summarizes the interaction among oxygen vacancy, CO gas and diffusing O^{2-} ions over YSZ grains. This equation explains well the carbon deposition around YSZ grain in Fig. 17 and the formation of oxygen gas in Figs. 10 and 13. Furthermore, the adsorption of O_2 molecules on produced carbon may explain the enriched concentration of oxygen atoms near the area of carbon deposition in Fig. 17. The oxygen atom at the oxygen lattice site diffuses to produce again oxygen vacancy by Eq. (26). Summation of Eqs. (25) and (26) provides Eq. (27) for the decomposition of CO into C and O_2 over YSZ grains through the interaction of CO-positively charged oxygen vacancy-diffusing oxide ions system. The above reaction mechanism is different from the CO decomposition mechanism at the cathode proposed in Fig. 16 and is possible in the anode layer and the porous electrolyte layer containing YSZ grains. The two reaction mechanisms in Figs. 16 and 18 are responsible for the electrochemical decomposition of CO in the porous YSZ cell. The proposed C deposition mechanism in Fig. 18 explains also

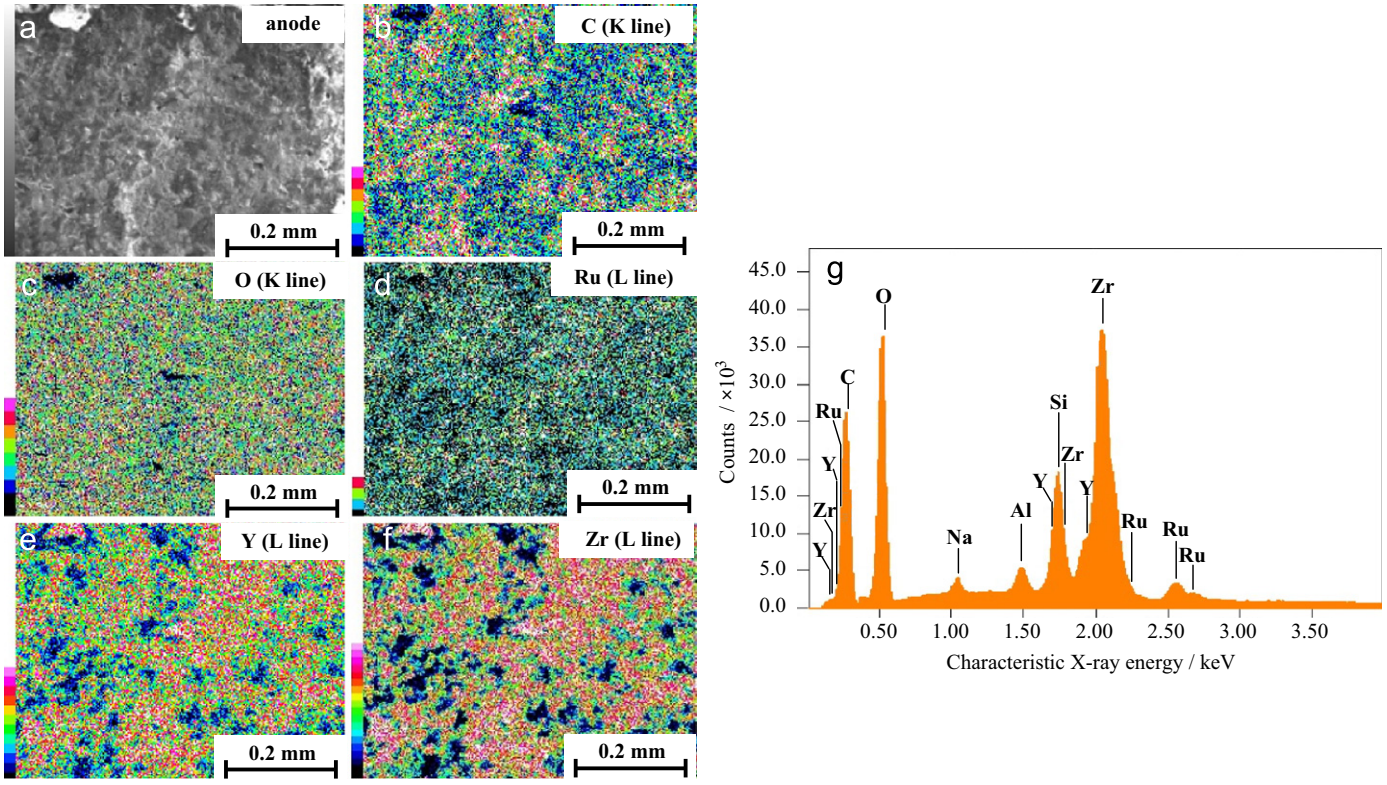

Fig. 15. (a) Microstructure of the Ru–YSZ anode after CO decomposition at 800 °C for 5 h, elementary distribution map of (b) C (K line), (c) O (K line), (d) Ru (L line), (e) Y (L line) and (f) Zr (L line), and (g) energy dispersive X-ray spectra at the Ru–YSZ anode.

Cathode

$$2CO + 2Ni \rightarrow 2NiO + 2C \quad (13)$$

$$2NiO + 4e^- \rightarrow 2Ni + 2O^{2-} \quad (14)$$

(13)+(14)

$$2CO + 4e^- \rightarrow 2C + 2O^{2-} \quad (15)$$

Anode(I)

$$2O^{2-} \rightarrow O_2 + 4e^- \quad (16)$$

Anode(II)

$$Ru + 2O^{2-} \rightarrow RuO_2 + 4e^- \quad (17)$$

$$RuO_2 + 2CO \rightarrow Ru + 2CO_2 \quad (18)$$

(17)+(18)

$$2O^{2-} + 2CO \rightarrow 2CO_2 + 4e^- \quad (19)$$

Anode(I) + Anode(II)

fraction, y (1-y)

$$2yO^{2-} \rightarrow yO_2 + 4ye^-$$

$$2(1-y)O^{2-} + 2(1-y)CO \rightarrow 2(1-y)CO_2 + 4(1-y)e^-$$

$$2O^{2-} + 2(1-y)CO \rightarrow yO_2 + 2(1-y)CO_2 + 4e^- \quad (20)$$

Total, (15) + (20)

$$2(2-y)CO \rightarrow 2C + yO_2 + 2(1-y)CO_2 \quad (21)$$

Fig. 16. Electrochemical decomposition mechanism of CO gas through porous YSZ cell.

the formation of C in Figs. 6 and 7 during CO_2 decomposition. A part of CO produced by Eq. (2) in Fig. 8 is decomposed over YSZ grains through the reaction by Eq. (25).

4. Conclusions

Electrochemical decomposition of CO_2 and CO gases were studied using a porous cell of Ru–YSZ anode/porous YSZ electrolyte/Ni–YSZ cathode system at 400–800 °C under 0.91–1.0 V/cm of electric field strength. The supplied CO_2 gas is decomposed to CO and O^{2-} ions at the cathode by the interaction with the supplied electrons. The formed CO and O^{2-} ions react again to form CO_2 and electrons at the anode, leading to no change of inlet CO_2 gas. However, a part of CO formed at the cathode reacts with Ni to form NiO and C. The O^{2-} ions corresponding to the deposited carbon are changed to O_2 gas and oxide compound of RuO_2 at the anode. The fraction of outlet gas was 61–63% CO_2 and 37–39% O_2 at 700–800 °C at a flow rate of 3 ml/min of outlet gas, and 73–96% CO_2 and 4–27% O_2 at 800 °C at a flow rate 50 ml/min at 800 °C. On the other hand, the supplied CO gas was decomposed to solid carbon, O_2 and CO_2 gases at 800 °C. No oxidation of Ni and Ru metals was confirmed. The fraction of outlet gas at 800 °C at a flow rate of 50 ml/min was 11–36% CO, 59–81% O_2 and 2–9% CO_2. The direct decomposition of CO into solid C and O_2 gas occurs through the following two different reaction mechanisms. The supplied CO gas is decomposed to solid C and O^{2-} ions over charged Ni metal at the cathode under a small DC electric field. The produced O^{2-} ions are discharged at the anode to produce O_2 gas and CO_2 gas by the reaction with CO gas conveyed to the anode. Another decomposition reaction of CO occurs over YSZ grains through the interaction of CO gas-positively charged oxygen vacancy of YSZ-diffusing oxide ions system. The supplied CO gas reacts with the

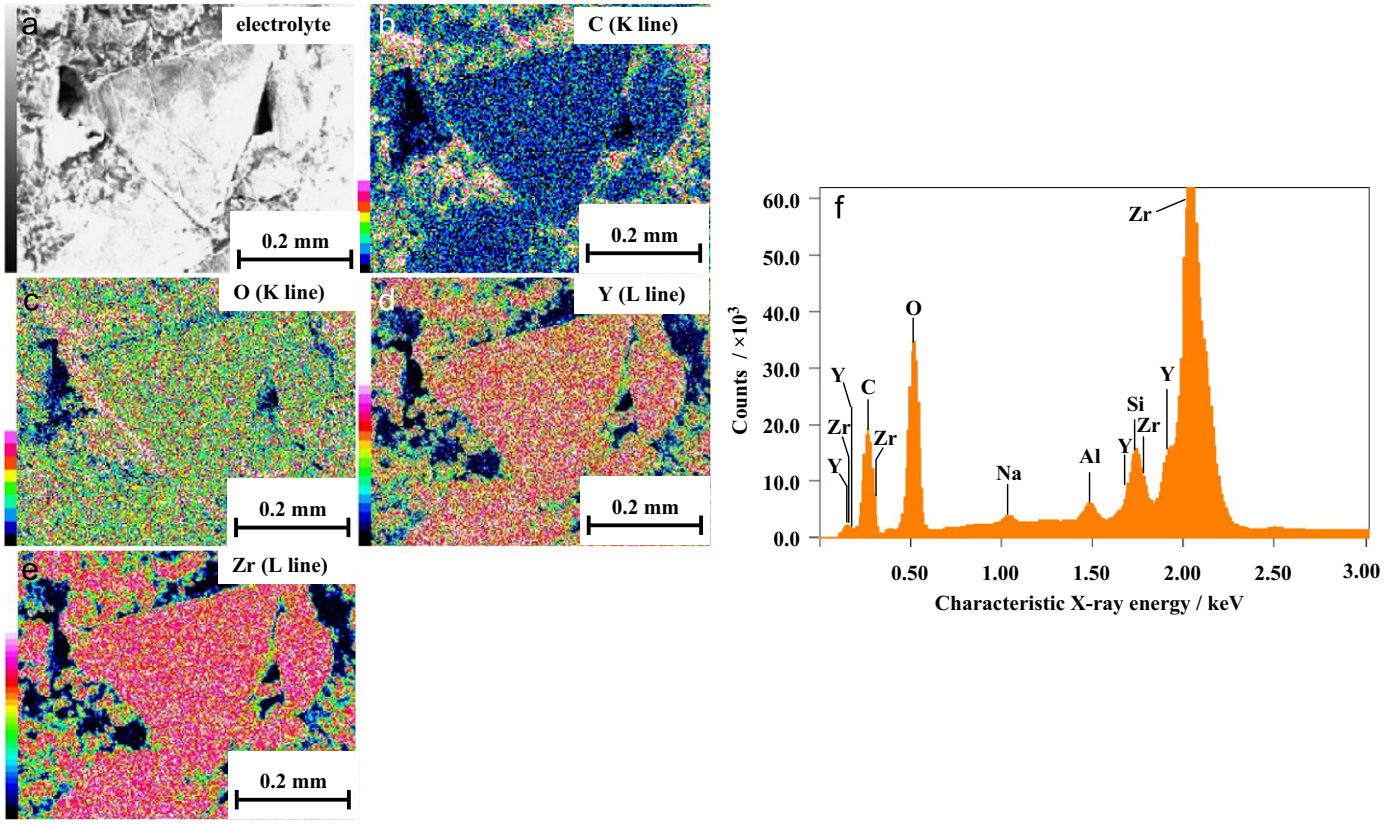

Fig. 17. (a) Microstructure of porous YSZ electrolyte after CO decomposition at 800 °C for 5 h, elementary distribution map of (b) C (K line), (c) O (K line), (d) Y (L line) and (e) Zr (L line), and (f) energy dispersive X-ray spectra at the YSZ electrolyte.

a

$$2Y_2O_3 \xrightarrow{4ZrO_2} 4Y_{Zr}' + 6O_O^{\times} + 2V_O^{\cdot\cdot} \quad (22)$$

$$2V_O^{\cdot\cdot} + 2CO \rightarrow 2O_O^{\times} + 2C + 4h^{\cdot} \quad (23)$$

$$4h^{\cdot} + 2O^{2-} \rightarrow O_2 \quad (24)$$

(23)+(24) $$2V_O^{\cdot\cdot} + 2CO + 2O^{2-} \rightarrow 2O_O^{\times} + 2C + O_2 \quad (25)$$

$$2O_O^{\times} \rightarrow 2V_O^{\cdot\cdot} + 2O^{2-} \quad (26)$$

Total, (25)+(26) $$2CO \rightarrow 2C + O_2 \quad (27)$$

b

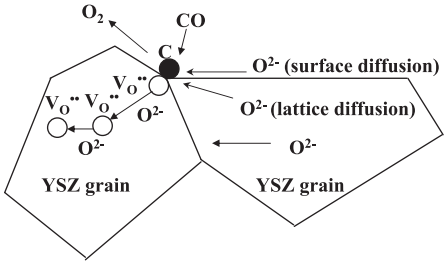

Fig. 18. (a) CO decomposition mechanism over YSZ grains under DC field and (b) scheme of the interaction among oxygen vacancy-CO gas-diffusing O^{2-} ions system over YSZ grains.

positively charged oxygen vacancy, which is produced by substitution of Zr ions for Y ions, to form solid carbon, lattice oxygen and holes. Since little hole conduction occurs in YSZ electrolyte, the produced holes react immediately with oxide ions transported from the cathode to form O_2 gas. The above two reaction mechanisms are responsible for the electrochemical decomposition of CO into C, O_2 and CO_2. The latter decomposition of CO over YSZ grains proceeds on the porous YSZ electrolyte and Ru–YSZ anode during the electrochemical decomposition of CO_2 gas.

References

[1] K. Sayama, K. Mukasa, R. Abe, Y. Abe, H. Arakawa, Stoichiometric water splitting into H_2 and O_2 using a mixture of two different photocatalysts and an IO_3^-/I^- shuttle redox mediator under visible light irradiation, Chemical Communications 23 (2001) 2416–2417.

[2] S. Sato, T. Arai, T. Morikawa, K. Uemura, T.M. Suzuki, H. Tanaka, T. Kjino, Selective CO_2 conversion to formate conjugated with H_2O oxidation utilizing semiconductor/complex hybrid photocatalysts, Journal of the American Chemical Society 133 (2011) 15240–15243.

[3] Y. Hirata, Y. Terasawa, N. Matsunaga, S. Sameshima, Development of electrochemical cell with layered composite of the Gd-doped ceria electronic conductor system for generation of H_2–CO fuel through oxidation–reduction of CH_4–CO_2 mixed gases, Ceramics International 35 (2009) 2023–2028.

[4] S. Matayoshi, Y. Hirata, S. Sameshima, N. Matsunaga, Y. Terasawa, Electrochemical reforming of CH_4–CO_2 gas using porous Gd-doped ceria electrolyte with Ni and Ru electrodes, Journal of the Ceramic Society of Japan 117 (2009) 1147–1152.

[5] Y. Hirata, N. Matsunaga, S. Sameshima, Reforming of biogas using electrochemical cell, Journal of the Ceramic Society of Japan 119 (2011) 763–769.
[6] M. Ando, Y. Hirata, S. Sameshima, N. Matsunaga, Electrochemical reforming of CH_4–CO_2 mixed gas using porous yttria-stabilized zirconia cell, Journal of the Ceramic Society of Japan 119 (2011) 794–800.
[7] Y. Hirata, Y. Tanaka, Proceedings of 6th Pacific Rim Conference on Ceramic and Glass Technology, The American Ceramic Society, CDR, 2006.